2007

Microstructural transformations and mechanical properties of cast NiAl bronze: Effects of fusion welding and friction stir processing

ELSEVIER

Materials Science and Engineering A 463 (2007) 128–137

MATERIALS SCIENCE & ENGINEERING A

www.elsevier.com/locate/msea

Microstructural transformations and mechanical properties of cast NiAl bronze: Effects of fusion welding and friction stir processing

M.D. Fuller [1], S. Swaminathan, A.P. Zhilyaev [2], T.R. McNelley *

Department of Mechanical and Astronautical Engineering, Naval Postgraduate School, Monterey, CA 93943-5146, USA

Received 30 March 2006; received in revised form 21 July 2006; accepted 22 July 2006

Abstract

A plate of as-cast NiAl bronze (NAB) material was sectioned from a large casting. A six-pass fusion weld overlay was placed in a machined groove; a portion of the weld reinforcement was removed by milling and a single friction stir processing (FSP) pass was conducted in a direction transverse to the axis of and over the weld overlay. A procedure was developed for machining of miniature tensile samples and the distributions of strength and ductility were evaluated for the fusion weld metal; for the stir zone (SZ) produced by the friction stir processing; and for a region wherein friction stir processing had taken place over the fusion weld. A region of low ductility in the heat affected zone (HAZ) of the fusion weld and in the thermomechanically affected zone (TMAZ) of friction stir processed material was attributed to partial reversion of an equilibrium lamellar eutectoid constituent upon local heating above ~800 °C and formation of non-equilibrium transformation products upon subsequent cooling. The adverse effect on ductility is worse in the heat affected zone of the fusion weld than in the thermomechanically affected zone of friction stir processing due to the lower heat input of the latter process. The implications of this work to engineering applications of friction stir processing are discussed.
Published by Elsevier B.V.

Keywords: NiAl bronze; Transformations; Welding; Friction stir processing; Microstructure–mechanical property relationships

1. Introduction

Cast NiAl bronze (NAB) alloys are widely used for large engineering components in marine applications due to useful combinations of strength, toughness and corrosion resistance. The physical metallurgy of NAB alloys is complex and a wide range of transformation products form during cooling depending on the details of the thermal history. During casting of large components the cooling rates encountered are often of the order of 10^{-3} K s^{-1}; accordingly the bcc β phase formed during solidification transforms to the fcc primary α phase with a Widmanstätten morphology beginning at about 1030 °C [1–8]. At 930 °C, nucleation of globular κ_{ii}, which is nominally Fe_3Al with a DO_3 structure, starts in the β phase. When the temperature reaches 860 °C, fine κ_{iv} precipitates, which are also nominally Fe_3Al, begin to form in the α phase. The remaining β decomposes by the eutectoid reaction $\beta \rightarrow \alpha + \kappa_{iii}$ at about 800 °C, resulting in the formation of a lamellar constituent. The κ_{iii} is nominally NiAl with a B2 structure; proeutectoid κ_{iii} may exhibit a globular morphology, or may form by epitaxy on the globular κ_{ii}. When the cooling rates are increased to around ~1 K s^{-1}, or greater, the rapid cooling suppresses the eutectoid reaction and, so, the Widmanstätten morphology of the α as well as bainitic and martensitic products of β phase decomposition may become apparent.

Casting porosity reduces physical properties and service performance, and is a common problem in cast NAB. Fusion welding (FW) is often used to fill casting porosity or otherwise repair and join these alloys, but can also induce its own defects that include porosity albeit on a relatively finer scale than in slowly cooled castings. An alternative approach to control the porosity as well as to enhance the mechanical properties of NAB is to use friction stir processing (FSP), which is a solid-state processing technology that provides localized modification and control of microstructure in processed regions of components. FSP has been employed successfully to close porosity in cast metals and to homogenize and refine microstructures in both cast and wrought metals, including alloys of Al [9–14] and Mg [15,16] and higher melting alloys of Cu [17–19], Fe [20] and

* Corresponding author. Tel.: +1 831 656 2589; fax: +1 831 656 2238.
E-mail address: tmcnelley@nps.edu (T.R. McNelley).
[1] Formerly student; currently with the U.S. Navy.
[2] On leave from the Institute for Metals Superplasticity Problems, Ufa, Russia.

0921-5093/$ – see front matter. Published by Elsevier B.V.
doi:10.1016/j.msea.2006.07.157

Ti [21]. Significantly improved strength/ductility combinations [22,23] and high-strain-rate superplasticity [10,12,13,24] have been achieved by FSP of wrought materials.

FSP is an allied process of friction stir welding (FSW) wherein a cylindrical, wear-resistant tool consisting of a smaller diameter pin with a concentric, larger-diameter shoulder is rotated and forced into the surface of the work piece. As the tool penetrates, a combination of frictional and adiabatic heating softens the material so that tool rotation induces a stirring action and flow of material about the pin. The severe, but localized, plastic deformation results in the formation of a stir zone (SZ) characterized by the presence of steep strain, strain rate and temperature gradients. Adjacent regions that experience only moderate straining comprise the thermomechanically affected zone (TMAZ). Just below the TMAZ is the heat affected zone (HAZ) where the material experiences rapid heating and cooling; this zone is akin to the HAZ of a FW.

By judicious choice of consumables and welding procedures the strength and ductility of as-deposited weld metal can be made to equal or exceed the corresponding base metal properties. Usually, these properties are evaluated by testing of tensile samples comprising only weld metal. During FSP of a cast metal the microstructure is converted from a cast to a wrought condition despite the absence of macroscopic shape change. Thus, improved tensile properties (relative to base metal) have been attributed to FSP although these properties are, again, generally evaluated by samples comprising only stir zone material. Nevertheless, in either FW or FSP of cast NAB there will be gradients in microstructure and properties. In particular, local gradients in the SZ and TMAZ strains and strain rates, as well as in temperatures, will result in gradients in mechanical properties in material processed by FSP.

It is the purpose of this report to investigate tensile properties as a function of location, from weld metal into base metal for a FW and from the SZ into base metal of NAB alloys subjected to FSP. To achieve this objective, a miniature tensile specimen was designed with dimensions sufficiently small to enable the variation in properties to be determined as a function of location in these various different zones. With the help of accurate registry, the tensile properties were then correlated to the corresponding microstructures. By comparing the variation in properties for FW and FSP the thermomechanical effects associated with FSP may be identified. Finally, in engineering applications, it is likely that FSP may be conducted over an existing FW region. Here, the microstructure and mechanical properties of FSP performed over a FW overlay of NAB were also documented.

2. Experimental procedures

The nominal composition of the C95800 material examined in this investigation is given in Table 1, which also provides the base metal composition for the plate used in this study. The plate had been sectioned from a large casting and had the following dimensions: length, 329 mm; width, 149 mm; thickness, 35 mm. A groove 16 mm in width and 6 mm in depth was machined along the center of the plate in the longitudinal direction (the x direction in Fig. 1). Gas metal arc welding (GMAW) process was used to place six passes in the groove using a Miller Delta Weld 651 CV machine, Ar shielding gas and Ampcotrode 46 weld filler wire 1.6 mm in diameter. The nominal wire composition corresponds to that of the as-cast NAB (Table 1). Each welding pass extended along the entire length of the plate and required ∼90 s to complete; ∼60 s elapsed between successive weld passes. The multi-pass GMAW weld is illustrated in the schematic of Fig. 1 and the welding pass sequence is shown in the inset.

The weld reinforcement was removed from one-half of the length of the plate by milling and a single FSP pass was conducted on the resulting surface using a Densimet 76 step-spiral tool with a pin depth of 6.3 mm. The tool rotation rate was 1000 rev. min^{-1} (RPM) and traversing rate was 76.2 mm min^{-1}. As shown in Fig. 1, the FSP pass was in a direction perpendicular to the axis of the weld, i.e., along the positive y direction, with the tool rotating counterclockwise about the z axis, as indicated by the curved arrow. The total distance of the FSP traverse was ∼120 mm such that the midpoint of the FSP traverse corresponded to the weld centerline. The FW and FSP were both

Table 1
Typical chemical composition range of as-cast UNS C95800 NAB, actual composition of as-cast NAB used in the present study provided by NSWC, Carderock Division, and chemical composition range of the weld electrode (Ampcotrode 46)

Element	C95800 (nominal composition)	Base metal chemistry	Ampcotrode 46[a] (nominal composition)
Copper	79 (minimum)	81.8	Balance
Aluminum	8.5–9.5	8.72	8.5–11.0
Nickel	4.0–5.0	4.31	4.0–6.0
Iron	3.5–4.5	3.59	3.0–5.0
Silicon	0.10 (maximum)	0.42	0.10 (maximum)
Manganese	0.8–1.5	1.41	0.60–3.50
Tin	–	0.017	
Carbon	–	0.007	
Sulfur	–	0.003	
Phosphorus	–	0.011	
Lead	0.03 (maximum)	0.0029	
Tungsten	–	<0.002	
Others			0.50 (maximum)

[a] Data obtained from www.unibraze.com/DataSheets/DataAlBrA4.pdf.

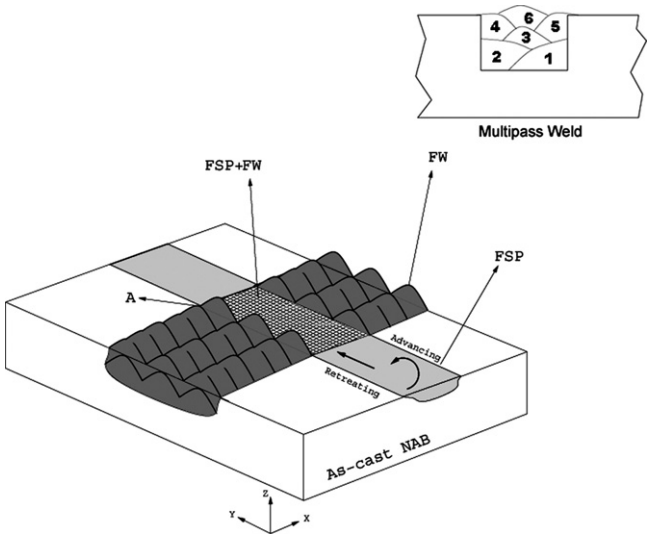

Fig. 1. Schematic of FW and FSP process performed on the as-cast NAB. Also shown is the schematic of the multi-pass FW operation. At point 'A', the tool exits the retreating side from the base material to the weld material.

accomplished at the Naval Surface Warfare Center, Carderock Division, Bethesda, MD.

Miniature tensile samples were obtained from base material, weld metal or stir processed material using a Charmilles Andrew EF630 electric discharge machine (EDM) employing consumable brass cutting wire with a nominal diameter of 0.3 mm. The tensile sample design is summarized in Fig. 2(a); the sample dimensions correspond to ASTM E-8 standards. Each tensile sample was lightly ground using the Buehler ECOMET 4 polishing wheel and a sequence of 400, 1000, 2400 and 4000 grit SiC paper to remove any cutting damage. Flatness of the tensile specimens was assured prior to mechanical testing. The tensile specimens were then examined using optical and stereo microscopy for defects, i.e., cracks, voids, etc., which could potentially affect the results of mechanical testing. The small size of these samples relative to the size of either the weld metal deposits or the FSP stir zone enables the spatial variations in properties, including ductility, to be resolved by mechanical testing. Fig. 2(b) is a schematic illustration showing the distribution of tensile samples throughout a process zone. The samples are represented by rectangles reflecting the gage cross section; a transverse view of a process zone shows that sample

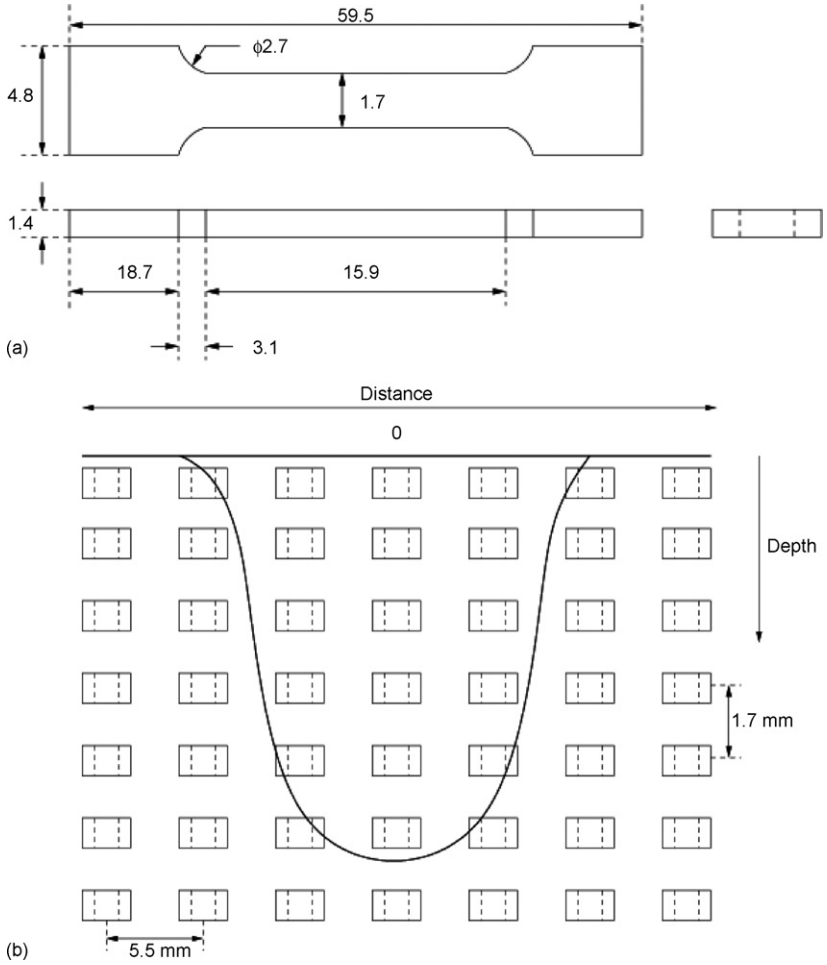

Fig. 2. (a) Schematic of miniature tensile specimen prepared from different regions of NAB subjected either to FSP or FW or combination of FSP and FW. All dimensions are given in millimeters. Actual thickness of tensile specimens varied based on metallographic preparation required to remove stress concentrators. (b) Schematic showing distribution of tensile specimens in and around the process zone.

blanks were removed by EDM and then individual samples were sliced from these blanks. In the current investigation the tensile axes were parallel to the welding direction for samples from FW material; parallel to the direction of tool advance for FSP; and parallel to the welding direction for the region of FSP over a FW. A computer-controlled INSTRON Model 4507 testing machine was used to perform all tensile testing. The gage width and thickness were measured prior to testing and samples were pulled to failure at a constant cross head displacement rate (1.1 mm min^{-1}) and the engineering stress versus engineering plastic strain curve was calculated from the recorded load versus time data. Fracture surfaces were characterized using a Topcon SM510 scanning electron microscope (SEM) operating with a tungsten filament.

Samples for microscopic analysis were metallographically prepared by standard methods. After polishing they were etched for 1–2 s in a solution of 40 ml water–40 ml ammonium hydroxide–2 ml hydrogen peroxide (30%), rinsing in water, followed by immersion for 1–2 s in a solution of 60 ml water–30 ml phosphoric acid–10 ml hydrogen peroxide. The etched samples were observed using bright-field (BF) illumination in a Zeiss Jenaphot 2000 equipped with a digital imaging system.

3. Results

3.1. Microstructure and mechanical properties of the fusion weld metal

Microscopy results from both longitudinal and transverse sections of the FW are shown in Fig. 3. Montages in Fig. 3(a) illustrate weld metal microstructures from the plate surface downward into base metal for the longitudinal and transverse sections; the transverse section shows the weld reinforcement build-up on both sides of the machined groove. Details of the solidified weld metal microstructure at locations 1 (near the weld surface) and 2 (along the centerline at the depth of the initial passes) are shown at higher magnification in Fig. 3(b). The Widmanstätten morphology of the α is evident at both locations but the microstructure is clearly finer at the depth of location 2. This likely reflects increasing base plate temperature and lower cooling rates during the later weld passes, and correspondingly longer solidification times at location 1. In both locations the dark-etching constituent is a bainitic or martensitic transformation product of the β. Three different sites along the fusion boundary (designated location 3) show a fine Widmanstätten morphology of α in the weld metal; in locations such as 3-ii a partially melted zone and cellular growth in the weld metal may be discerned. The dark-etching constituent in the HAZ (marked by arrows in Fig. 3((b) 3-i and 3-ii)) at all sites along the fusion line is a bainitic or martensitic transformation product of β. At locations 3-i and 3-iii, this constituent is at the fusion line; the formation of this constituent reflects local peak temperatures above the eutectoid temperature (800 °C) followed by cooling at a rate sufficient to enable formation of non-equilibrium transformation products of β. At location 3-ii, only partial reversion of the lamellar $\alpha + \kappa_{iii}$ has occurred and the bainitic or martensitic transformation product of the resulting β has formed within the lamellar structure. The micrograph from location 4 shows the base metal microstructure. Fine κ_{iv} particles are dispersed in primary α while the lamellar $\alpha + \kappa_{iii}$ constituent and coarse κ_{ii} particles are apparent in between the primary α grains.

The results of tension testing for the FW region are summarized in Fig. 4(a). The EDM procedure enabled samples to be obtained from the plate surface to a depth of 25 mm below the surface and, so, the variation in properties through the weld metal, HAZ and onward into base metal could be evaluated. Inspection of data from locations more than 10 mm below the plate surface reveals yield strengths of ∼200 MPa, tensile strengths of ∼400 MPa and ductility values of ∼10% elongation to failure. These values are consistent with tensile data for slowly cooled NAB castings. The yield and tensile strengths of the weld metal vary somewhat with location in the weld. A peak in these strength measures is apparent about 5 mm below the plate surface at a location corresponding to the interface between the first and second layers of weld metal. The ductility is also higher for tensile samples from within the weld metal; the average properties within the weld metal (yield strength ∼400 MPa; tensile strength ∼600 MPa; ∼18% elongation to fracture) correspond well with published data for such welds.

While the strength data decrease smoothly from the weld metal through the HAZ and onward into base metal there appears to be a distinct ductility minimum for locations corresponding to the HAZ. This is especially apparent at locations underneath the weld reinforcement to either side of the weld, where ductility fell to 2–3% elongation to failure. Nevertheless, low ductility values were apparent at all locations in the HAZ along the fusion line. The crack profile for a HAZ sample (∼4% elongation to failure) beneath the weld along the weld centerline is shown in the inset in Fig. 4(b). The microstructure data from the deformed gage section of this sample show partial dissolution of the lamellar $\alpha + \kappa_{iii}$ constituent that is similar to that of location 3-ii along the fusion boundary in Fig. 3(b). The fracture surface of this sample exhibits a mixture of a brittle cleavage mode associated with cracking of the partially dissolved eutectoid constituent, and microvoid formation and coalescence, as shown in Fig. 4(c). Corresponding fractography from a base-metal sample that gave ∼10% elongation to failure is shown in Fig. 4(d); a similar mixture of modes is evident in this sample as well.

3.2. Microstructure–mechanical property relationships for FSP

A montage of optical micrographs for a transverse section from FSP of the NAB is shown in Fig. 5(a). The advancing side is to the right-hand side while the retreating side is to the left-hand side of this image. The microstructure is highly refined throughout most of the SZ and an ‘onion ring’ pattern is evident along the SZ centerline. The onion ring pattern may reflect material drawn from different locations on successive tool rotations by the tool spiral features and then brought together upon passage of the tool [19]. The microstructure at location 3 corresponds to a region in the SZ just below the bottom of the tool pin and thus reflects material that had experienced less severe deforma-

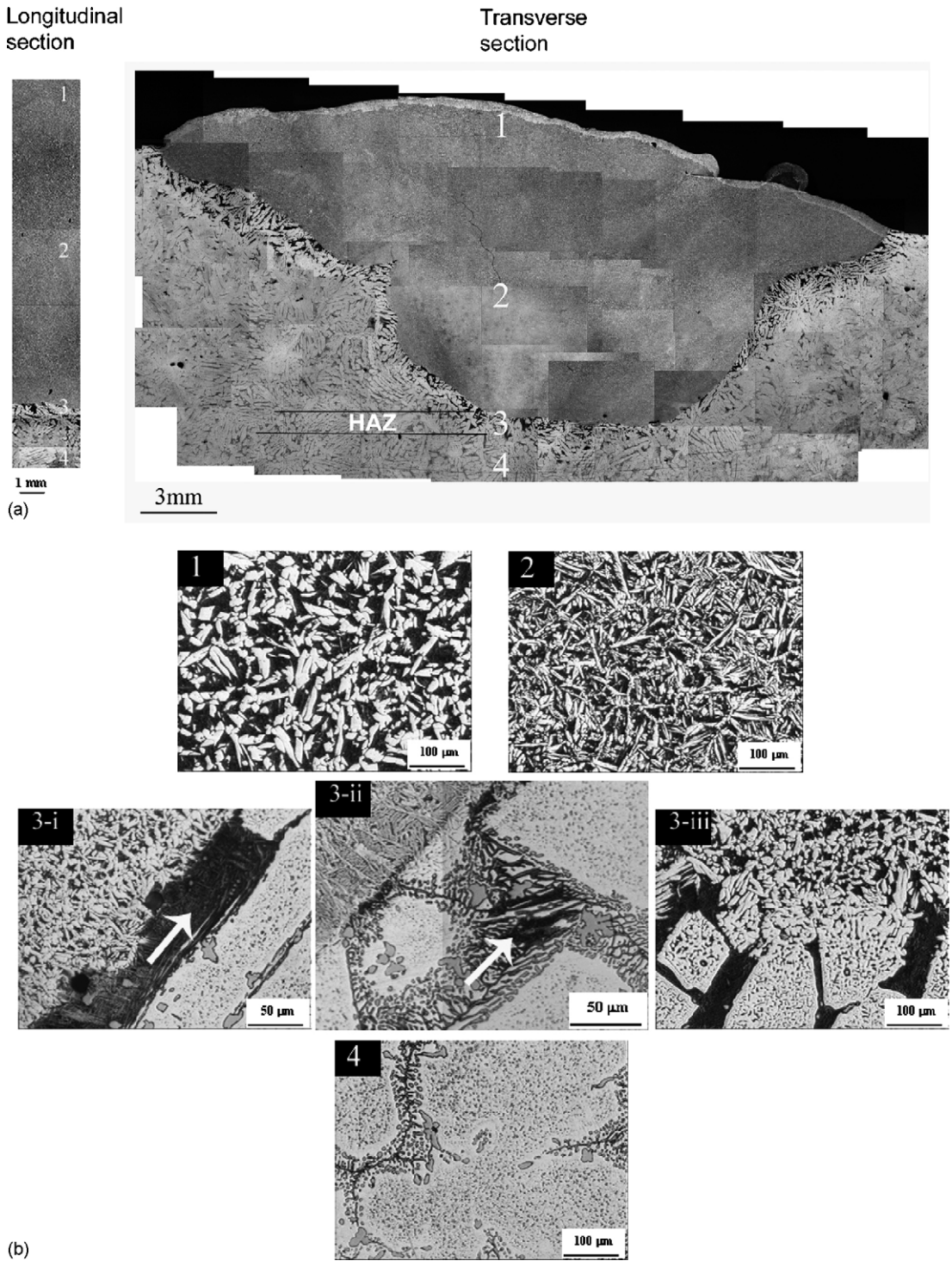

Fig. 3. (a) Optical microscopy montage of longitudinal and transverse view of NAB subjected to FW. (b) Higher magnification optical microscopy images taken from different regions of NAB as marked in (a). Sub-parts (3-i to 3-iii) refer to microscopy performed on different regions along the periphery of the weld zone or the HAZ.

tion than locations higher in the SZ. The interface between the SZ and TMAZ is distinct on the advancing side of the tool and more diffuse under the tool and on the retreating side. The dark-etching bainitic or martensitic constituent is evident everywhere in the TMAZ; distortion of the TMAZ is also evident although the local sense of shear appears to vary along the SZ–TMAZ interface.

More detail of the microstructures at the various locations indicated in the montage of Fig. 5(a) is provided in the micrographs of Fig. 5(b). The distinct Widmanstätten morphology evident in the weld metal is not apparent in this SZ. Instead, location 1 shows elongated α grains intermingled with dark-etching β transformation products. Because this material formed from base metal during the severe FSP thermomechanical cycle

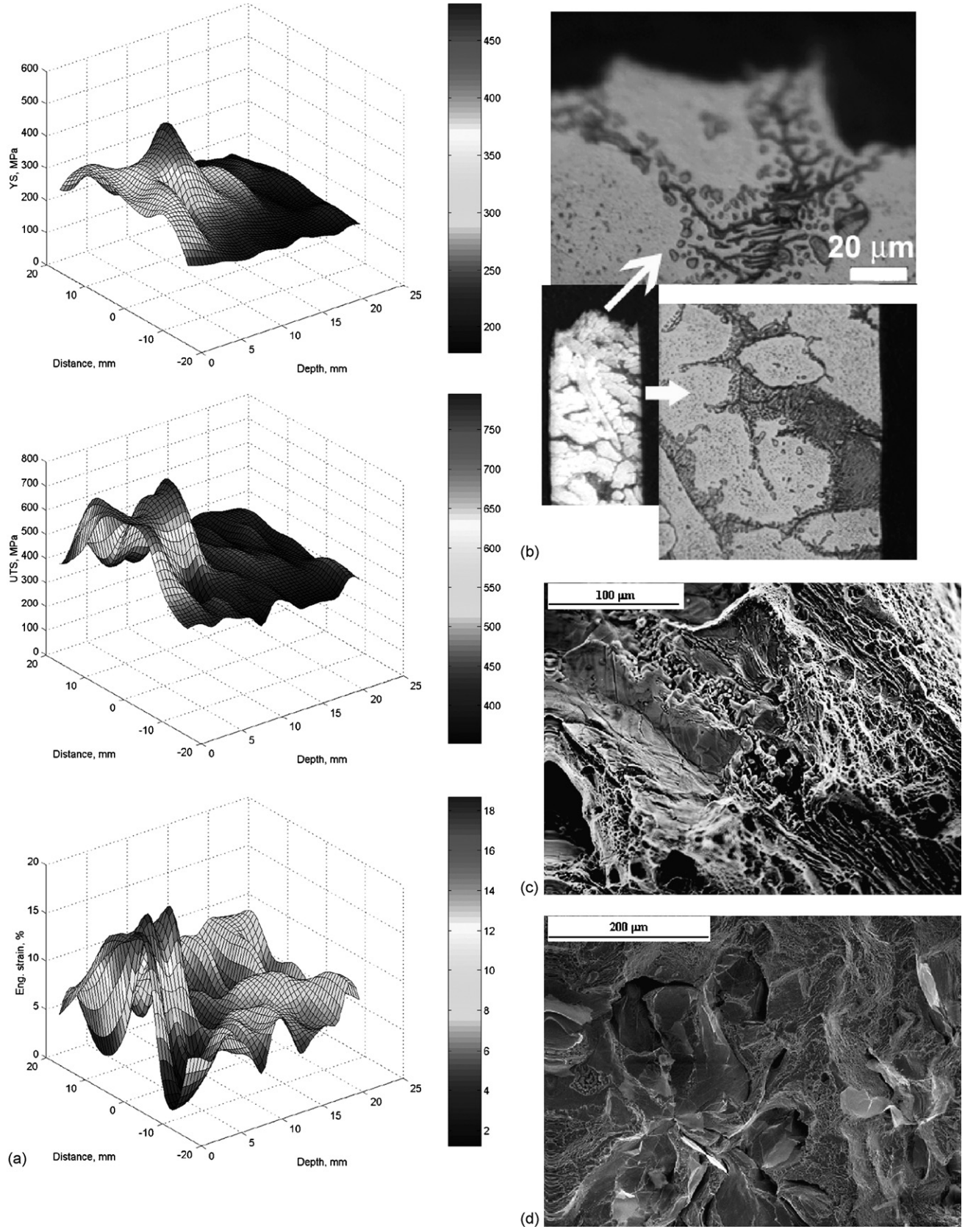

Fig. 4. (a) Contour plots showing spatial variation of YS, UTS and ductility in NAB subjected to FW as determined from miniature tensile specimens. (b) Optical microscopy image of a fracture surface profile of a tensile specimen along the center line just below the weld line showing evidence of partial dissolution of lamellar $\alpha + \kappa_{iii}$ and transformation products of β. (c) SEM fractograph associated with (b) showing both cleavage mode associated with cracking of the partially dissolved eutectoid constituent and microvoid formation and coalescence. (d) SEM fractograph of the base material, having a ductility of 10%, that also shows a mixture of brittle cleavage mode and microvoid formation.

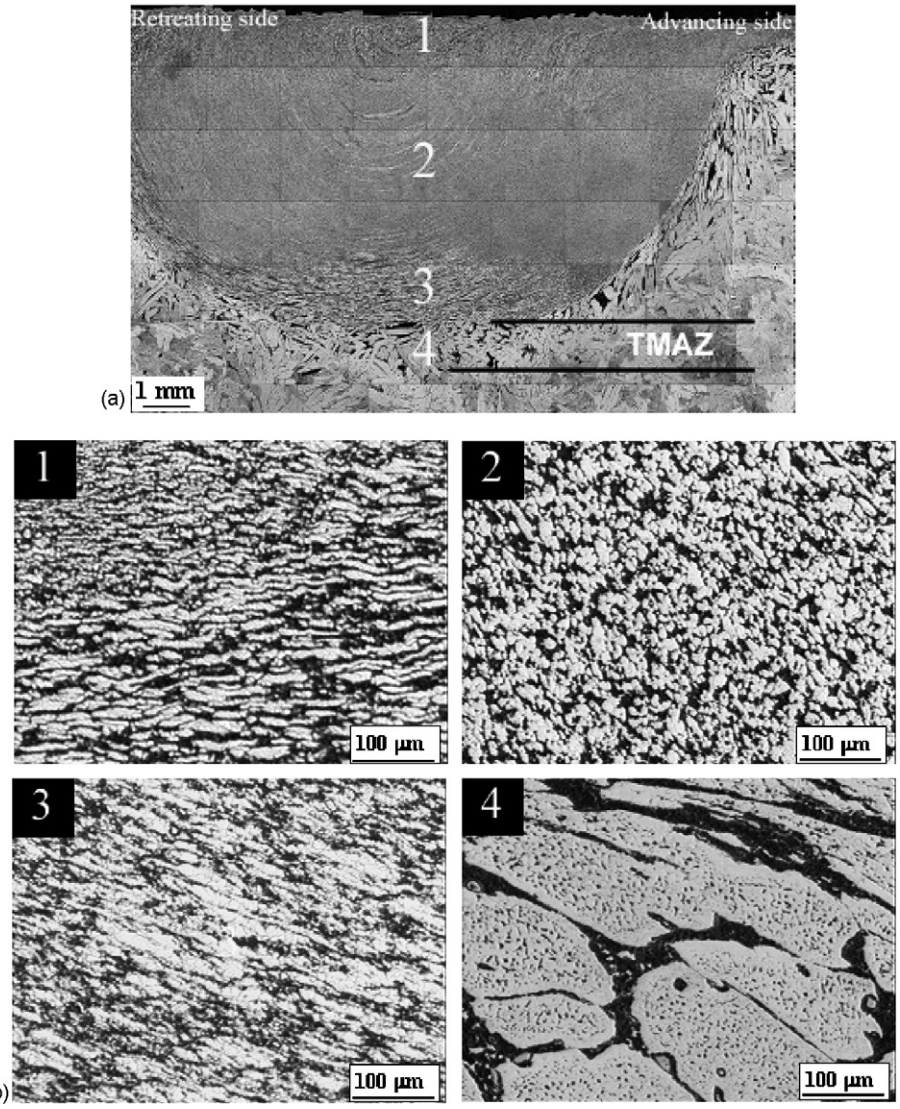

Fig. 5. (a) Optical microscopy montage of NAB subjected to FSP. (b) Higher magnification images from different regions marked in (a).

the occurrence of β transformation products indicates that this location in the SZ had experienced heating and deformation at temperatures greater than 800 °C, thereby causing the eutectoid reversion reaction $\alpha + \kappa_{iii} \rightarrow \beta$ to occur [18,19]. Location 2 is within the distinct onion ring pattern although this pattern is not obvious in the higher magnification micrograph for this location in Fig. 5(b). Both α grains and β transformation products are apparent but the α grains are more nearly equiaxed in shape in location 2 when compared to location 1. In location 3 near the bottom of the tool pin and beneath the 'onion ring' pattern the microstructure again comprises of elongated α grains and β transformation products but the α grains are greater in size while the volume fraction of β transformation products is less than in location 1. This is consistent with less strain and lower peak temperatures at locations low in the SZ [19].

Details of the TMAZ (location 4) are also provided in Fig. 5(b). The primary α grains exhibit some distortion but are similar in size to those of base metal and the κ_{iv} remains undissolved. The lamellar eutectoid constituent has disappeared and been replaced by dark-etching products of the β transformation during rapid cooling; this microstructure suggests that the α and β phases have undergone compatible deformation at a temperature above the eutectoid, 800 °C, but below the κ_{iv} solvus, 860 °C, in the TMAZ.

The distribution of mechanical properties for the FSP region is summarized in Fig. 6(a). Comparison of the FW and FSP data indicate that these FSP conditions give a SZ yield strength of 450–500 MPa, which is slightly higher than the weld metal yield strength, and a similar tensile strength of ~600 MPa. The tensile ductility varied with location in the SZ but remained above base metal ductility. These data show that ductility was at a minimum for samples in the TMAZ under the tool shoulder or elsewhere in the TMAZ along the SZ–TMAZ interface. Nevertheless, the adverse effect of FSP on TMAZ ductility was not as severe as the adverse effect of FW on HAZ ductility for this NAB material. Fractography data in Fig. 6(b) that was obtained from a SZ sample shows a predominance of microvoid formation and coalescence after 18% elongation to fracture. In contrast, the

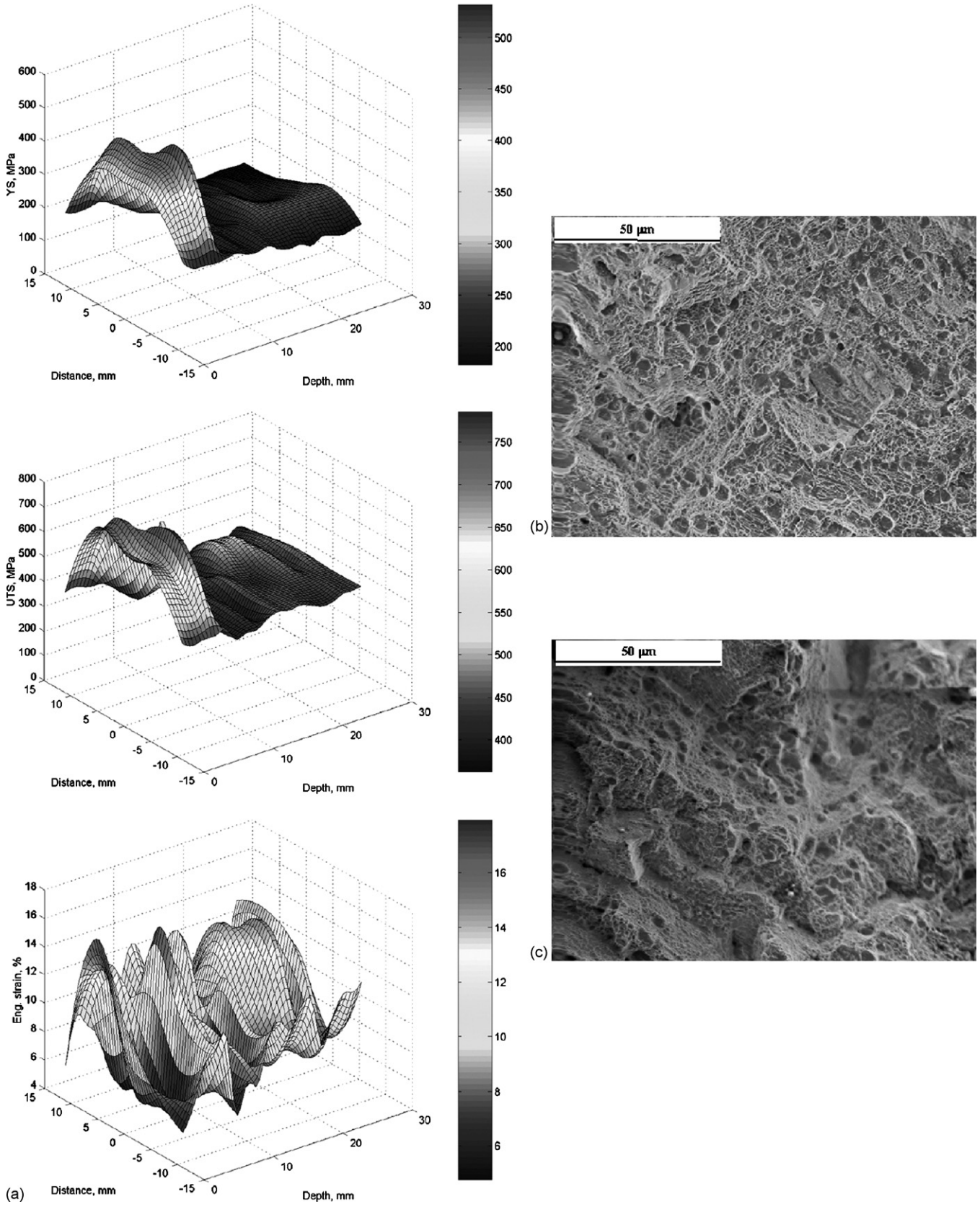

Fig. 6. (a) Contour plots showing spatial variation of YS, UTS and ductility in NAB subjected to FSP as determined from miniature tensile specimens. SEM fractograph: (b) from inside the stir zone showing ductile type fracture and (c) of a tensile specimen from SZ–TMAZ interface showing microvoid formation and brittle cracking.

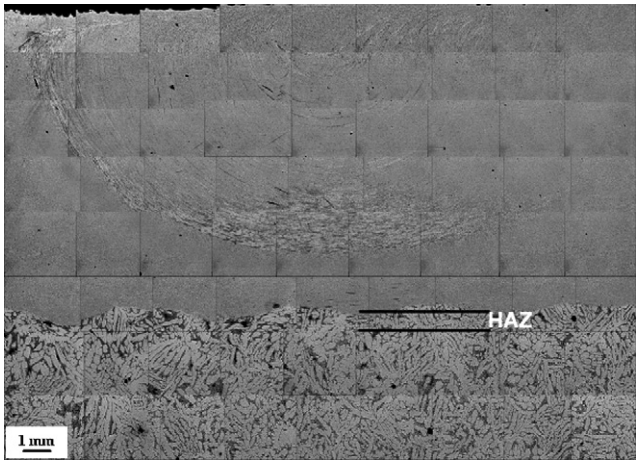

Fig. 7. Optical microscopy montage of NAB subjected to FSP over a FW near the center of the weld. Higher magnification images, to the most part, resemble the corresponding regions reported in Figs. 3(b) and 5(b).

fractography obtained from the SZ–TMAZ interface (Fig. 6(c)) shows a mixture of microvoid formation and cracking that may reflect separation along the interface between the deformed primary α and the bainitic or martensitic transformation product of the β.

3.3. Microstructure–mechanical property data for FSP over a FW

A montage showing a transverse section from the FSP pass that had been performed over the FW overlay is shown in Fig. 7. A detailed examination revealed that the SZ of the FSP region was very similar in structure to the SZ from FSP of the base metal. The TMAZ was indistinct in this region while the HAZ of the weld metal was identical in nature to the HAZ observed in the longitudinal section of the FW shown in Fig. 3(a).

The distributions of strength and ductility in this region are summarized in the contour plots of Fig. 8. The SZ yield and tensile strengths in this case is slightly higher (up to 500 and 750 MPa, respectively) than the corresponding SZ yield and tensile strengths for FSP through base metal. Tensile ductility within the SZ was also consistent with SZ ductility for FSP through base metal. However, a location of low ductility under the tool shoulder on the retreating side was observed in this case. This is location A in Fig. 1 on the retreating side where the tool exits the weld metal and passes back into base metal. Metallographic analysis is not conclusive but suggests that there is a complex pattern reflecting the interaction of the retreating side of the tool on the interface between weld metal and base metal.

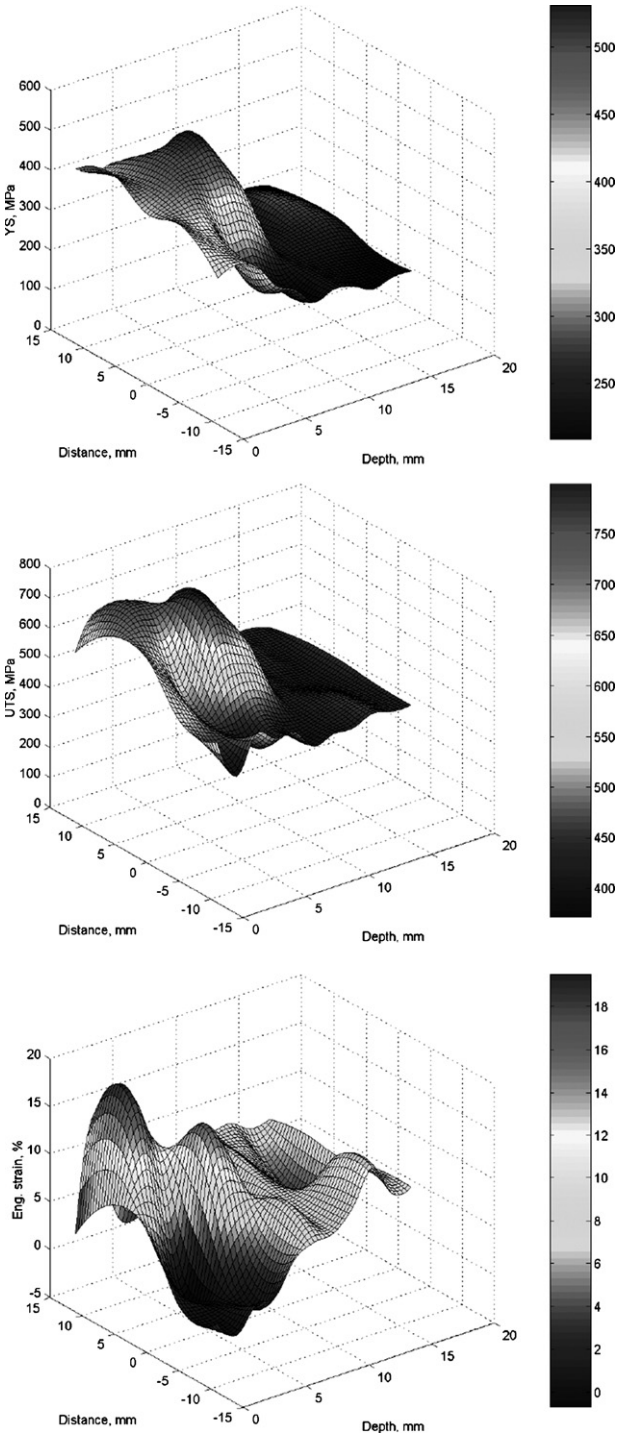

Fig. 8. Contour plots showing spatial variation of YS, UTS and ductility in NAB subjected to FSP over FW.

4. Discussion

Slowly cooled cast NAB exhibits an equilibrium structure consisting mainly of coarse primary α and a lamellar decomposition product resulting from the reaction $\beta \rightarrow \alpha + \kappa_{iii}$. In turn, the primary α contains a fine dispersion of Fe_3Al (κ_{iv}) while a coarser dispersion of Fe_3Al (κ_{ii}) is present in the eutectoid. This NAB material typically contains significant porosity. The cooling rates during conventional GMAW are sufficient to suppress the eutectoid reaction and result in weld metal microstructures that comprise α with a Widmanstätten morphology and various non-equilibrium transformation products of β. Such microstructures exhibit both higher strength and ductility than the slowly cooled base metal. This likely reflects a combination of microstructure refinement and a lesser porosity content

in weld metal when compared to the base metal. Nevertheless, there is a distinct region of low ductility in the HAZ of the weld wherein fracture appears to initiate in transformation products of β formed in unmelted base during the welding thermal cycle.

The thermomechanical cycle of FSP results in homogenization and refinement of the NAB in the SZ. The extent of refinement and nature of the SZ microstructures depend sensitively on FSP parameters such as the tool design, pin depth and the combination of RPM and traversing rate. Parameters leading to high peak SZ temperatures (e.g., approaching 1000 °C) appear to produce strength–ductility combinations well in excess of those of weld overlays. The material of the current investigation appears to have an aluminum content on the low side of the allowed composition range for C95800 NAB and, so, direct application of the temperature estimation procedures reported in earlier work on a 9.5 wt.% Al alloy is not feasible [19]. Nevertheless, the large volume fraction of deformed primary α and absence of SZ Widmanstätten α here is consistent with lower peak temperatures (i.e., $T_{Peak} \leq 900\,^{\circ}C$) during FSP. Resulting mechanical properties reflect a combination of grain refinement in the primary α, strengthening by dispersions of undissolved κ phases and β transformation products, and strain hardening. The TMAZ of FSP also exhibits β transformation products due mainly to the thermal cycle in the TMAZ. As in FW, these products are associated with reduced ductility, although the adverse effect of ductility here is not as pronounced as observed in association with FW. This may reflect that FW typically involves higher heat inputs than FSP due to melting of filler wire and subsequent deposition of the molten metal.

When FSP is performed over an existing FW overlay, enhanced strength and ductility of NAB are observed in the stirred region (Fig. 8). However, there also exists a region showing low ductility at the point where the retreating side of the SZ moves from weld metal into base metal. This location is presently under investigation. Furthermore, in engineering applications FSP will be conducted using rastering or spiral patterns that have been shown to eliminate undesirable microstructures after multiple passes [23].

5. Conclusions

(i) A combination of β transformation products and finer α grains produces a region of enhanced strength and ductility in NAB alloys subjected to FSP or FW.
(ii) There exists a zone along the HAZ in FW and the TMAZ in FSP wherein the material displays lower ductility due to partial reversion of the lamellar $\alpha + \kappa_{iii}$ to β, and the formation of bainitic or martensitic transformation products of the β during subsequent cooling.

Acknowledgements

The processed materials were provided by Ms. Jennifer Nguyen and Dr. David Forrest of the Naval Surface Warfare Center, Carderock Division, Bethesda, MD. Funding for this work was provided by the Defense Advanced Research Projects Agency (DARPA), with Dr. Leo Christodoulou as program monitor, and the Office of Naval Research (ONR), with Dr. Julie Christodoulou as program monitor.

References

[1] E.A. Culpan, G. Rose, Br. Corros. J. 14 (1979) 160.
[2] G.M. Weston, Survey of Nickel-Aluminum Bronze Casting Alloys for Marine Applications, Australia Department of Defence Report DSTO MRL-R807, Melbourne, 1981.
[3] P. Brezina, Int. Met. Rev. 27 (1982) 77.
[4] E.A. Culpan, G. Rose, J. Mater. Sci. 13 (1978) 1647.
[5] F. Hasan, A. Jahanafrooz, G.W. Lorimer, N. Ridley, Metall. Trans. A 13 (1982) 1337.
[6] F. Hasan, G.W. Lorimer, N. Ridley, J. Phys. 43 (C4) (1982) 653.
[7] A. Jahanafrooz, F. Hasan, G.W. Lorimer, N. Ridley, Metall. Trans. A 14 (1983) 1951.
[8] P. Weill-Couly, D. Arnaud, Fonderie 322 (1973) 123.
[9] R.S. Mishra, M.W. Mahoney, S.X. McFadden, N.A. Mara, A.K. Mukherjee, Scr. Mater. 42 (2000) 163.
[10] R.S. Mishra, M.W. Mahoney, Mater. Sci. Forum 357–359 (2001) 507.
[11] Z.Y. Ma, R.S. Mishra, M.W. Mahoney, Acta Mater. 50 (2002) 4419.
[12] I. Charit, R.S. Mishra, Mater. Sci. Eng. A359 (2003) 290.
[13] Z.Y. Ma, R.S. Mishra, M.W. Mahoney, R. Grimes, Mater. Sci. Eng. A351 (2003) 148.
[14] Y.S. Sato, M. Urata, H. Kokawa, Metal. Mater. Trans. 33A (2002) 625.
[15] S.H.C. Park, Y.S. Sato, H. Kokawa, Scr. Mater. 49 (2003) 161.
[16] D. Zhang, M. Suzuki, K. Maruyama, Scr. Mater. 52 (2005) 899.
[17] H.S. Park, T. Kimura, T. Murakami, Y. Nagano, K. Nakata, M. Ushio, Mater. Sci. Eng. A371 (2004) 160.
[18] K. Oh-ishi, T.R. McNelley, Metall. Mater. Trans. A 35A (2004) 2951.
[19] K. Oh-ishi, T.R. McNelley, Metall. Mater. Trans. A 36A (2005) 1575.
[20] Y.S. Sato, T.W. Nelson, C.J. Sterling, Acta Mater. 53 (2005) 637.
[21] A.P. Reynolds, E. Hood, W. Tang, Scr. Mater. 52 (2005) 491.
[22] M.W. Mahoney, W.H. Bingel, S.R. Sharma, R.S. Mishra, Mater. Sci. Forum 426 (2003) 2843.
[23] K. Oh-ishi, A.P. Zhilyaev, R. Williams, T.R. McNelley, in: K.V. Jata, M.W. Mahoney, R.S. Mishra, T.J. Lienert (Eds.), Friction Stir Welding and Processing III, TMS, Warrendale, PA, 2005, p. 107.
[24] I. Charit, R.S. Mishra, Acta Mater. 53 (2005) 4211.